Microchimica Acta (2023) 190:180
https://doi.org/10.1007/s00604-023-05711-4

ORIGINAL PAPER

Fast cathodic electrodeposition of ZnTCPP-functionalized metal–organic framework films for preparation of a fluorescent aptamer sensor for microcystin determination

Chang Su[1] · Ding Jiang[2,3] · Shuyong Jia[1,4] · Xueling Shan[2,3] · Zhidong Chen[1,3]

Received: 7 November 2022 / Accepted: 19 February 2023 / Published online: 12 April 2023

Abstract

A one-step electrodeposition-assisted self-assembly technique has been developed for preparation of ZnTCPP@MOF films with three-dimensional mesoporous structure in a three-electrode system. The internal structure of the ZnTCPP@MOF films was tuned by adjusting the electrochemical deposition voltage, deposition time, and the concentration of ZnTCPP at room temperature. The ZnTCPP@MOF films under different deposition conditions were characterized by scanning electron microscopy, Fourier transformation infrared spectroscopy, and X-ray photoelectron spectroscopy. The prepared ZnTCPP@MOF films exhibited excellent fluorescence properties, in which ZnTCPP molecules were encapsulated inside the MOF as fluorescent signal probes and structure-directing agents, which affected the electrochemical response of the ZnTCPP@MOF films. The sensing platform based on ZnTCPP@MOF film was used to detect microcystin with a wide determination range (1.0×10^{-12} mol/L ~ 1.0×10^{-5} mol/L), low determination limit (3.8×10^{-13} mol/L), and high sensitivity. More importantly, the strategy is simple, low-cost, green, and environmentally friendly, and it provides a new strategy for the direct use of MOFs films as signaling components.

Keywords Electrochemical deposition · ZnTCPP@MOF film · Fluorescent aptamer sensor · Self-assembly

Introduction

Our ecosystems and drinking water resources are not only vulnerable toward anthropogenic pollutants but also natural toxins. Among the natural toxins from diverse natural environments, cyanobacterial toxins produced by aquatic organisms pose a growing and serious threat for aquatic ecosystems and human health [1–4]. The most commonly reported cyanotoxins are microcystins (MCs), which are present in water bodies and have caused the deterioration of water quality [5, 6]. MC with leucine arginine (MC-LR) is the most frequently addressed member of the MC homolog, due to its abundance and potential toxicity [7]. The results of experiments have revealed that humans exposed to low concentration of MCs for long-term are apt to cause a rapid disorganization of the hepatic architecture. However, MC-LR has a cyclic structure and double bonds which enhance its stability and persistence in the environment, and almost impossible to be removed even by high-temperature boiling, so it has become an important pollutant in water quality control and environmental monitoring [8]. In 1998, the World Health Organization (WHO) has proposed 1 μg/L as a limiting value for MC-LR in drinking water [9], which promoted researchers to seek novel mechanisms for detecting MC-LR, and that provides positive and practical significance for early prevention and analysis.

In addition, several analytical methods have been developed for the determination of MC-LR in water, such as liquid chromatography–mass spectroscopy (LC–MS), high-performance liquid chromatography (HPLC), protein

✉ Zhidong Chen
zdchen@cczu.edu.cn

1 School of Materials Science and Engineering, Changzhou University, Changzhou 213164, Jiangsu, China

2 Jiangsu Key Laboratory of Advanced Catalytic Materials and Technology, School of Petrochemical Engineering, Changzhou University, Changzhou 213164, China

3 Advanced Catalysis and Green Manufacturing Collaborative Innovation Center, Changzhou University, Changzhou 213164, China

4 Lite-On OPTO Tech(CZ) Co., Ltd, No. 88, Yanghu Rd., Wujin Hi-Tech. Industrial Development Zone, Changzhou City, China

phosphatase inhibition assay (PPIA), and enzyme-linked immunosorbent assay (ELISA) [10, 11]. However, these analytical techniques have more or less disadvantages, such as requiring complex sample preparation, qualified personnel, and expensive equipment, which are laborious and time-consuming and not efficient. Therefore, it is necessary to develop a convenient, specific, and sensitive method for MC-LR detection. As compared to these methods, the method of fluorescence (FL) detection possesses the property of simple signal transduction, low instrumentation cost, absolute sensitivity, and relatively simple operation, which has been applied to diverse areas including water and food safety, medical diagnostics, and environmental pollutants [12–14]. Unfortunately, using FL alone is not sufficient to accurately select because of insufficient detection specificity. Various strategies have been studied to overcome this limitation. Aptamer is a single-stranded nucleic acid that was obtained by the systematic evolution of ligands employing exponential enrichment (SELEX) technology and could recognize many different targets with high affinity and strong specificity [15–17]. Thus, the aptamer is employed as the recognition moiety in sensors. At present, FL aptasensors, which combine the selective recognition of aptamers for testing substances with a series of advantages of FL, have been explored as a promising method for the specific and sensitive detection of MC-LR.

Fascinating and functionally underpinning metal–organic frameworks (MOFs) have opened up a versatile horizon, such as biomedical applications, chemical separation, and sensing, which attribute to their unique properties such as high agent loading, high volume of adjustable micropores, large surface area, and permanent open porosity [18, 19]. In order to implement these functional materials into practical applications, the better way is to synthesize them into thin films for practical applications rather than synthetic powders [20]. Previously, several methods for the synthesis of MOF films have been developed, including chemical vapor deposition, seeded growth, Langmuir – Blodgett layer-by-layer deposition, and electrochemical deposition [21, 22]. Among these, electrochemical deposition is a pioneering technology owing to their ease of synthesis even at room temperature. Furthermore, it is a kind of mild, fast, manageable normal position agreement, and MOF film can be directly grown on its conductive substrate [23, 24]. Unfortunately, most researches have been mainly focused on microporous MOF films, which have considerable disadvantages such as limited mass transfer and diffusion rates, low electrical conductivity, and low loading of guest molecules that challenge the practical applications of the MOF electrochemical systems [25, 26]. Fortunately, Nematollahi et al. developed a novel, selective, and environmentally friendly strategy for the fabrication of mesoporous MOF thin films via the electrochemical synthesis and deposition technique [27].

This strategy can provide a larger specific surface area and more active sites, thereby increasing the electron transport rate, enhancing the electrical conductivity, and also facilitating the entry of more guest molecules into the structure.

As is well known, porphyrins and their derivatives are a class of aromatic compounds, which possess numerous excellent properties, such as stable structure, abundant active sites, non-toxic, tunable band gap, intense visible-light absorption, and redox behavior [28, 29]. In recent years, there have been large numerous reports about porphyrins or metalloporphyrins used as organic ligands in the synthesis of MOFs [30, 31]. Yu et al. used zirconium chloride octahydrate and tetrakis (4-carboxyphenyl) to produce microporous Zr-based porphyrinic MOF-545 thin film on conducting glass substrates [32]. Ndjawa et al. produced microporous Zn-metallated MOF thin films based on the 5, 15-diphenyl-10, 3, 20-di(4-carboxyphenyl) porphyrin ligand by a facile liquid-phase epitaxy approach [33]. However, low loading of guest molecules and slow mass transfer are deficiencies of microporous MOFs along with low surface area. In this context, soft-templating or surfactant-templated approach has been directed toward resolving these problems [34].

In this work, we developed a novel strategy for in situ preparing zinc tetraphenyl porphyrin-functionalized metal–organic framework (ZnTCPP@MOF) films by using one-step electrochemical-assisted deposition technique. In this method, taking zinc(II) meso-5,10,15,20-tetrakis (4-carboxyphenyl) porphyrin (ZnTCPP) as the fluorescent signal probe and structure-directing agent, 1,3,5-benzenetricarboxylic acid (H_3BTC) as the organic ligand, and $Zn(NO_3)_2$ as the cation source, ZnTCPP@MOF thin film were synthesized on the surface of FTO by one-step electrodeposition and electrochemically driven synergistic reaction. Among them, by applying a voltage, OH^- was generated on the surface of the cathode electrode, and the pH of the electrode surface was changed. Therefore, the deprotonation of an organic ligand (H_3BTC^-) and the self-assembly of ZnTCPP on the surface electrode are due to electrostatic interaction. So a large number of ZnTCPP molecules were encapsulated in the cavities of the ZnTCPP@MOF thin film framework. The formed mesoporous ZnTCPP@MOF thin film framework could enhance the molecular load and conductivity. The encapsulation quantity of ZnTCPP controls the growth and crystallization process of MOF thin films, which affects the fluorescence properties of ZnTCPP@MOF thin films. Therefore, it exhibits excellent fluorescence-responsive performance as a sensing platform, the fluorescence of ZnTCPP@MOF thin films was quenched by the specific binding of aptamers to microcystin, and the

fluorescence intensity was linearly related to the concentration of MC-LR.

Experimental section

Reagents and materials

Absolute ethanol (C_2H_5OH), zinc nitrate hexahydrate ($Zn(NO_3)_2{\cdot}6H_2O$), and sodium carbonate ($NaNO_3$) were obtained from Sinopharm Chemical Reagent Co. Ltd (Shanghai, China). Omethoate, acetamiprid, microcystin-YR (MC-YR), microcystin-LA (MC-LA), and MC-LR were purchased from Sigma-Aldrich (Shanghai, China). Zinc(II) meso-5,10,15,20-tetrakis (4-carboxyphenyl) porphyrin (ZnTCPP) and trimesic acid (H_3btc) were purchased from Shanghai Chemical Reagent Co. Ltd. Microcystin-LR aptamer (5′- GGC GCC AAA CAG GAC CAC CAT GAC AAT TAC CCA TAC CAC CTC ATT ATG CCC CAT CTC CGC -3′) supplied by Shang Gong Biotech Co., Ltd (Shanghai, China) were dissolved in Tris–HCl buffer solution (pH 7.5, containing 20 mM Tris–HCl, 100 mM NaCl, 2 mM $MgCl_2$, and 5 mM KCl, 1 mM $CaCl_2$) and stored at 4 °C for use. All reagents were of analytical grade and used directly without any treatment. Besides, ultrapure water (18.2 MΩ) was utilized throughout the whole experiment. The purity of all reagents is more than 99%.

Instruments

Scanning electron micrograph (SEM) images of the materials was obtained using a JEOL scanning electron microscope (JSM-6360LA, Japan) and a JEOL transmission electron microscope (JEOL 2100, Japan), respectively. The fluorescence spectrum was detected on a Hitachi F-4500 fluorescence spectrophotometer (Tokyo, Japan). Fourier transform infrared spectroscopy (FT-IR) was performed using a Max-2000 (Rigaku Co., Ltd, Japan) and Nicolet IFn 10 (Thermo Fisher, USA), respectively. Electrochemical impedance spectroscopy (EIS) was performed on a ZENNIUM electrochemical workstation (Zahner Instruments, Germany) in 5.0 mM $Fe(CN)_6^{3-/4-}$ containing 0.1 M KCl solution.

Electrochemical deposition experiments were carried out on a CHI660E electrochemical workstation (Shanghai Chenhua Instrument, Co., Ltd) with a typical three-electrode cell. After polishing and sonication, the fluorine-doped SnO_2(FTO) ($1 \times 1 cm^2$) served as the working electrode. A platinum sheet electrode ($1 \times 1 cm^2$) and a KCl-saturated calomel electrode (SCE) were employed as the counter and reference electrodes, respectively.

The speed of stirring in all experimental procedures was 400 rpm.

Electrochemical deposition of the Zn-MOF thin films modified electrode

According to the literature [35], 1.33 g of $Zn(NO_3)_2{\cdot}6H_2O$ as a cation source and 0.127 g of $NaNO_3$ as a supporting electrolyte were dissolved in 15 mL of deionized water (solution A). Meanwhile, 0.525 g of H_3BTC was dissolved in 15 mL of ethanol (solution B). Solutions A and B were sonicated for 10 min and stirred for 15 min, respectively. Then, solution B was added to solution A under vigorous stirring to form a mixed solution. The pH of the solution was adjusted to 2.1 with HCl and stirred for 2.5 h to form a uniform electrolyte solution at room temperature.

The processed FTO was immersed in the above prepared solution, and the simultaneous synthesis and deposition of the Zn-MOF thin film were accomplished by applying a suitable potential (− 1.3 V vs SCE) for 1 h and a stirring rate of 400 rpm. The Zn-MOF/FTO electrode was finally rinsed with ultrapure water for further experiments.

Electrochemical deposition of two-dimensional ZnTCPP-MOF thin films modified electrode

1.33 g of $Zn(NO_3)_2{\cdot}6H_2O$ as a cation source and 0.127 g of $NaNO_3$ as a supporting electrolyte were dissolved in 15 mL of deionized water (solution A). Meanwhile, 3 mg of ZnTCPP were dissolved in 15 mL of ethanol (solution B). Solutions A and B were, respectively, sonicated for 10 min and stirred for 15 min. Then, solution B was added to solution A under vigorous stirring to form a mixed solution. The pH of the solution was adjusted to 2.1 with HCl and stirred for 2.5 h to form a uniform electrolyte solution at room temperature.

The processed FTO was immersed in the above prepared solution, and the simultaneous synthesis and deposition of the ZnTCPP@MOF thin film were accomplished by applying a suitable potential (− 1.3 V vs SCE) for 1 h and a stirring rate of 400 rpm. The ZnTCPP@MOF/FTO electrode was finally rinsed with ultrapure water for further experiments.

Electrochemical deposition of the three-dimensional ZnTCPP-functionalized MOF (ZnTCPP@MOF) thin films modified electrode

1.33 g of $Zn(NO_3)_2{\cdot}6H_2O$ as a cation source and 0.127 g of $NaNO_3$ as a supporting electrolyte were dissolved in 15 mL of deionized water (solution A). Meanwhile, 0.525 g of H_3BTC and 3 mg of ZnTCPP were dissolved in 15 mL of ethanol (solution B). Solutions A and B were, respectively, sonicated for 10 min and stirred for 15 min. Then, solution B was added to solution A under vigorous stirring to form a mixed solution. The pH of the solution

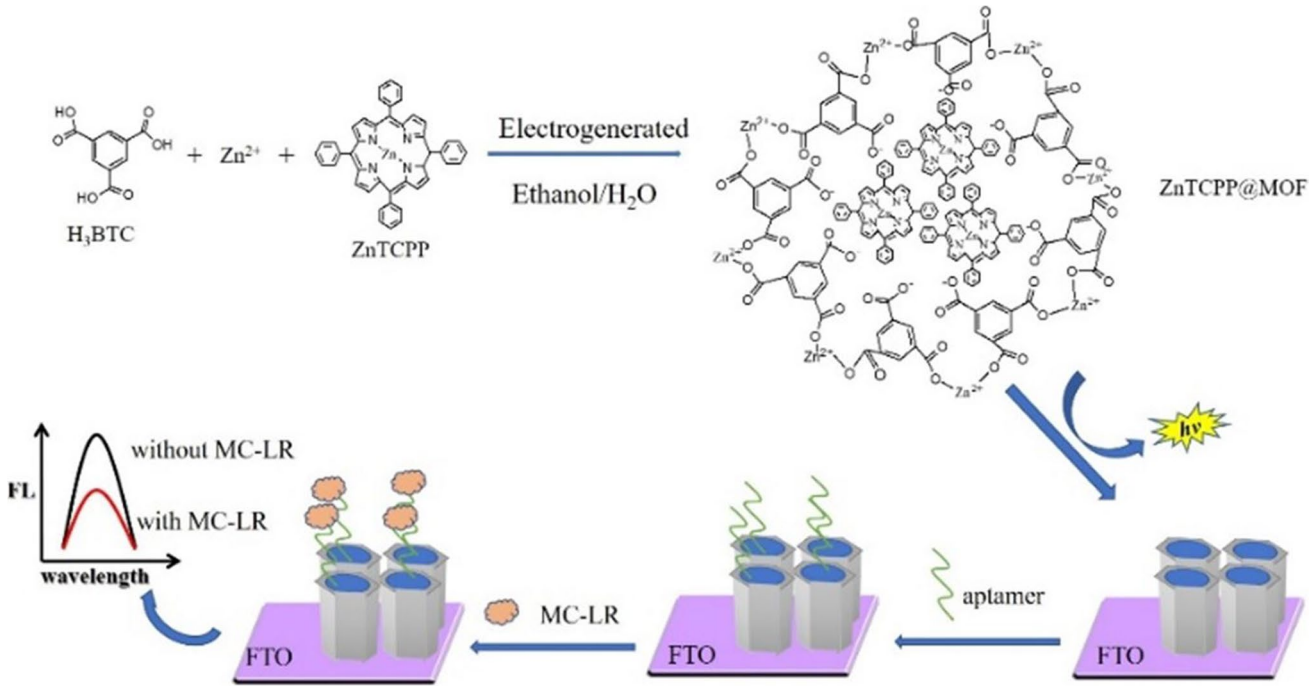

Scheme 1 Schematic diagram of the fabrication of ZnTCPP functional metal–organic frameworks modified electrode (ZnTCPP@MOF/FTO) and FL aptasensor construction

was adjusted to 2.1 with HCl and stirred for 2.5 h to form a uniform electrolyte solution at room temperature.

The processed FTO was immersed in the above prepared solution, and the simultaneous synthesis and deposition of the ZnTCPP@MOF thin film were accomplished by applying a suitable potential (− 1.3 V vs SCE) for 1 h and a stirring rate of 400 rpm. The ZnTCPP@MOF/FTO electrode was finally rinsed with ultrapure water for further experiments.

Preparation of FL aptamer sensors based on ZnTCPP@MOF films and MC-LR determination

As shown in Scheme 1, 20 µL of 2 µM aptamer solution was dropped on the ZnTCPP@MOF/FTO and dried the solution in air to obtain the apt/ZnTCPP@MOF/FTO, which was also called FL aptasensor. In the process of MC-LR detection, the apt/ZnTCPP@MOF/FTO was immersed in MC-LR solution for 40 min and the MC-LR/apt/ZnTCPP@MOF/FTO electrode. Then use the excitation wavelength of 310 nm to measure the FL of the FTO electrode and record the FL intensity of the emission wavelength at 368 nm, where F was the FL intensity of the apt/ZnTCPP@MOF-modified FTO without MC-LR and F_0 indicated the FL intensity in the presence of different concentrations of MC-LR and $\Delta F = F - F_0$.

Results and discussion

Characterization of ZnTCPP@MOF thin films

As shown in Scheme 1, the electrochemical strategy that was combined with self-assembly technology was employed for the fabrication of ZnTCPP@MOF thin films on the electrode surface. The electrodeposition bath was composed of $Zn(NO_3)_2$ as a Zn source, H_3BTC as an organic ligand, ZnTCPP as a fluorescent signal probe and a structure-directing agent, and $NaNO_3$ acted as a support electrolyte. Firstly, the three electrodes were immersed in the above-mentioned plating solution. Then, apply a voltage of − 1.3 V to generate OH − in situ on the surface of FTO electrode, resulting in an increase in the local pH of the electrode surface, causing the deprotonation of the neutral ligand. Finally, the negatively charged ligands and the positively charged fluorescent signal probe self-assemble into thin films on the FTO electrode by electrostatic interaction which could encapsulate the ZnTCPP in the cavities of MOF thin films. The stepwise electrogeneration of OH − is the key factor to control the ligand deprotonation and regulate the nucleation rate of MOF thin films on the electrode surface [36, 37]. Figure 1 shows that the thin films gradually grew from needles to flaky and finally to three-dimensional columns

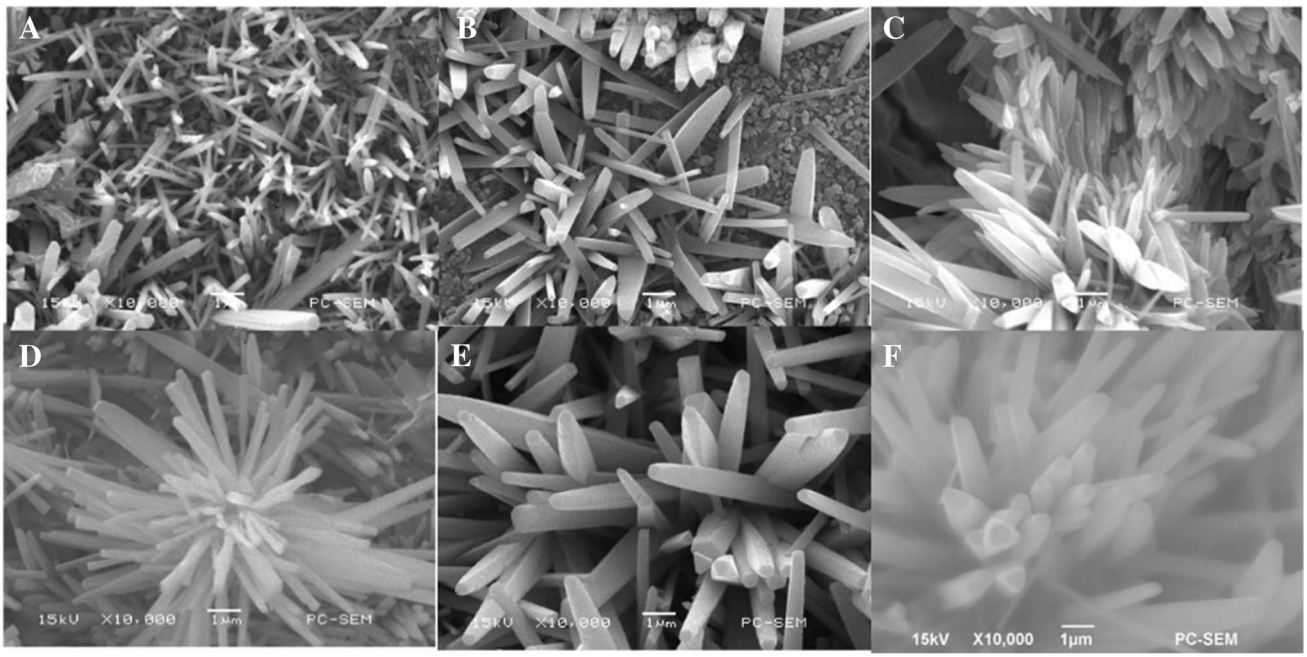

Fig. 1 SEM images of ZnTCPP@MOF films on the FTO at different electrodeposition times: **A** $t = 600$ s, **B** $t = 1200$ s, **C** $t = 1800$s, **D** $t = 2400$ s, **E** $t = 3000$ s, **F** $t = 3600$ s; electrodeposition potential: $E = -1.3$ V vs SCE

as the electrodeposition time was prolonged from 600 to 3600 s, because a longer deposition time could electrogenerate more OH^- and the thin film had enough time to grow to the peak of three-dimensional hexagon. Fig. S1 also reveals a high nucleation rate when the voltage was increased from − 1.0 to − 1.3 V and the crystal size gradually decreased. It may be that with the increased of deposition voltage, the formation rate of OH^- increased, so the nucleation rate was also accelerated, and more crystals could be generated faster, which caused the crystal size to become smaller.

At the same time, the concentration of ZnTCPP also could control the growth of thin films. As shown in Fig. S2, when the concentration of ZnTCPP was 0.05 mM, the crystals appeared as two-dimensional sheets, which are due to lack of enough ZnTCPP to combine with ligands. As the concentration of ZnTCPP increased to 0.15 mM, the crystals gradually grew into a three-dimensional columnar morphology. Therefore, ZnTCPP could act as a structure-directing agent, which could control the growth and structure morphology of MOF.

Fig. S3A also shows the structure of Zn-MOF without ZnTCPP as the structure-directing agent. It can be seen that Zn MOF presented a two-dimensional rod structure, which growth was horizontal and not perpendicular to the electrode surface. When the ZnTCPP directly replaced H_3BTC as the organic ligand, as shown in Fig. S4B, the morphology of ZnTCPP-MOF was filamentous. Those all indicated that the role of the ZnTCPP in ZnTCPP@MOF was a structure-directing agent.

To demonstrate that the Zn, N, and O elements were uniformly distributed in the MOFs polygon, we recorded the elemental mapping distributions of the MOF, as shown in Fig. 2. The Zn and O elements should come from ZnTCPP and $Zn(NO_3)_2$, and the N elements should come from ZnTCPP, which also proved that the ZnTCPP@MOF molecules were successfully composited.

We further performed Fourier transform infrared (FT-IR) characterization for the electrodeposited ZnTCPP@MOF. As shown in Fig. 3A, unlike free H_3BTC, the unique peaks of free COO^- and the carboxylic acid (3086–2552 cm^{-1}) disappeared in the ZnTCPP@MOF films, indicating that the combination of metal ions and organic ligands promoted the nucleation of MOFs. After ZnTCPP was encapsulated in MOF, the FT-IR spectra of ZnTCPP@MOF showed the absorption peaks of ZnTCPP itself in comparison with that of H_3BTC. XPS was also applied to illustrate the chemical composition of the ZnTCPP@MOF. As anticipated, the ZnTCPP@MOF is composed of Zn 2p, N 1 s, O 1 s, and C1s elements; these proofs demonstrated that the ZnTCPP complex was successfully doped in the MOFs synthesized.

Optimization of deposition conditions and sensor

In order to obtain a high fluorescence intensity, the deposition time, the deposition voltage, the concentration of ZnTCPP, the

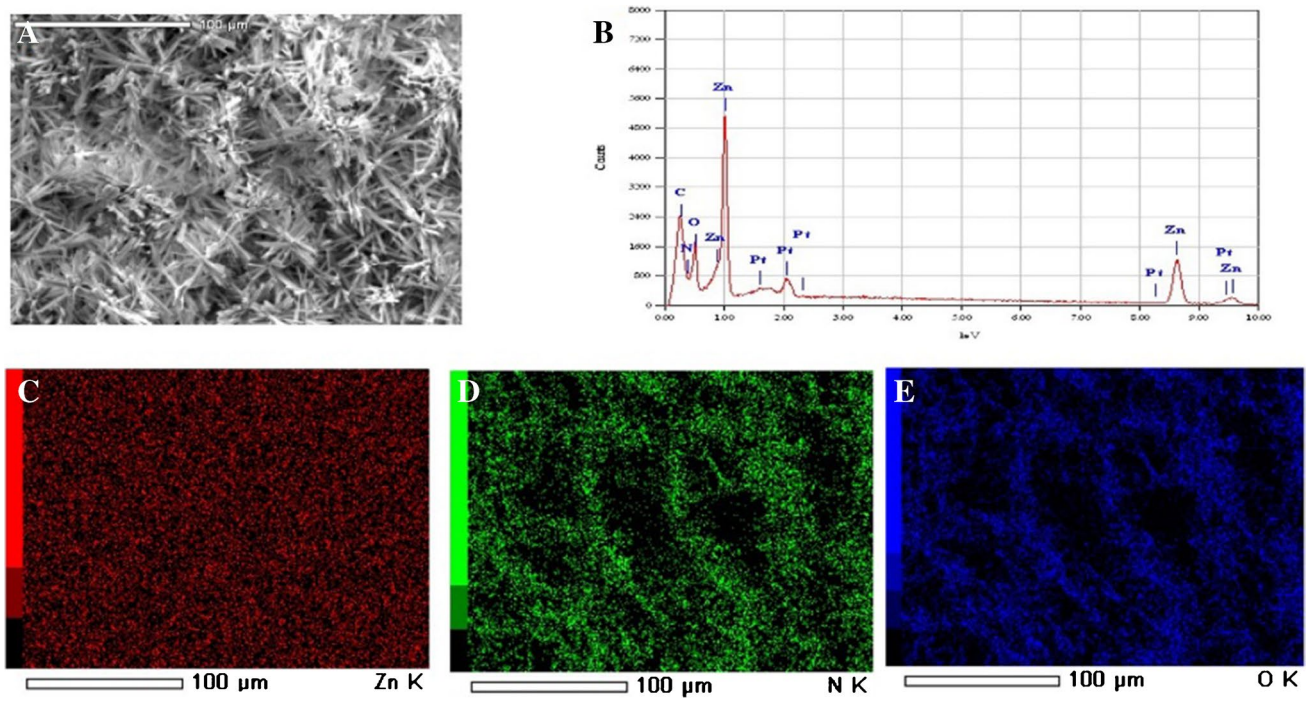

Fig. 2 **A** SEM images of ZnTCPP@MOF on the FTO and **B** its corresponding EDX spectra. **C**–**E** Elemental maps for Zn-K, N-K, and O-K, respectively. Electrolysis potential at the $E = -1.3$ V vs SCE and electrolysis time $t = 3600$ s

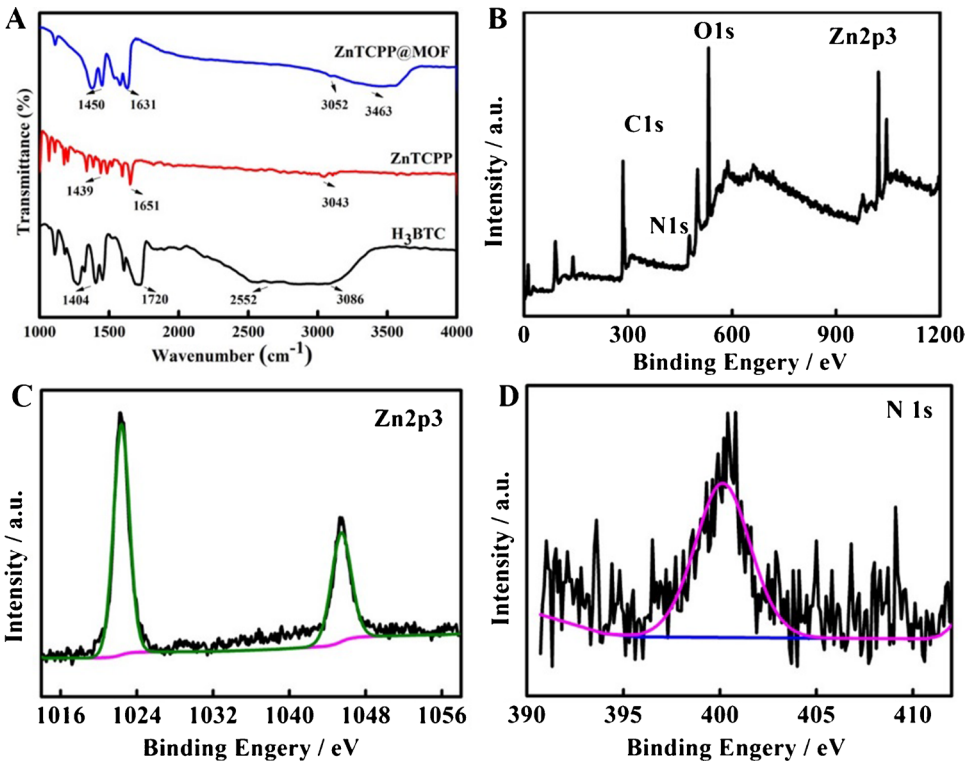

Fig. 3 FT-IR spectra of H_3BTC, ZnTCPP, ZnTCPP@MOF (**A**), XPS analysis for **B** the full region of XPS for ZnTCPP@MOF, **C** the Zn 2p region, **D** the N 1 s region

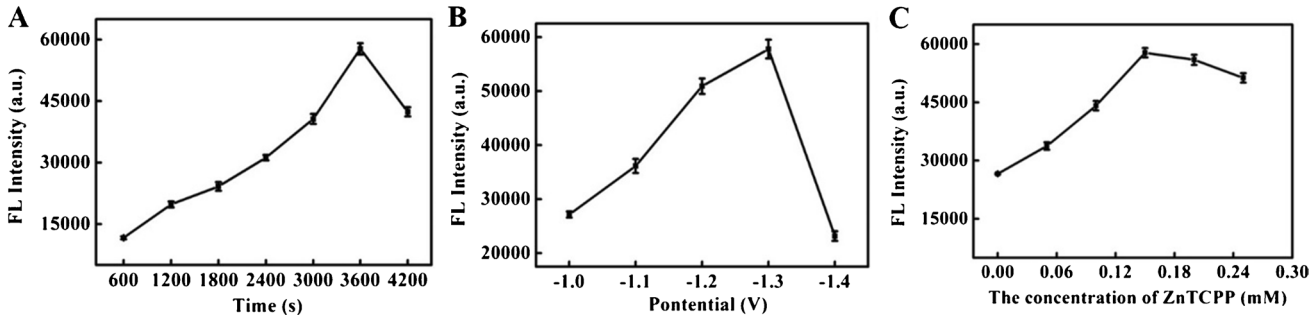

Fig. 4 **A** The influence of the electrodeposition times, **B** the electrodeposition voltages, **C** the concentration of ZnTCPP for the intensity of ZnTCPP@MOF thin film

concentration of aptamer, and the reaction time between the aptamer and MC-LR were optimized. In this method, the fluorescence signal probe molecule (ZnTCPP) was encapsulated in polyhedral MOF thin films, and the effects can be observed by changing the deposition time. As shown in Fig. 4A, as the increased of deposition time, more ZnTCPP molecules could be encapsulated within the MOFs, so the FL intensity enhanced continuously and reached its maximum at 3600 s. Yet, as the deposition time continued to extend (≥4200 s), the MOF thin films became thicker which were undesirable, and the fluorescence intensity was reduced. Thus, the optimum deposition time to synthesize MOF thin films was 3600 s.

The influence of deposition voltage on the fluorescence intensity of ZnTCPP@MOF thin film was presented in Fig. 4B, and the FL intensity grew gradually as the deposition voltage increased. The highest FL intensity was obtained when the deposition voltage was − 1.3 V. The FL intensity downed when the voltage exceeded − 1.3 V. This may be ascribed to the formation of metal zinc at higher voltage. Therefore, − 1.3 V was selected as the best deposition voltage.

Figure 4C depicted the effect of ZnTCPP concentration (0–0.25 mM) on the FL intensity of the ZnTCPP@MOF thin film. The FL intensities increased gradually with an increase in the concentration of ZnTCPP from 0 to 0.15 mM. However, as the concentration of ZnTCPP increased by more than 0.15 mM, the fluorescence intensity decreased, because too much ZnTCPP molecules in the precursor solution would compete with the organic ligand, which prevents the generation of ZnTCPP@MOF thin films. Therefore, 0.15 mM of ZnTCPP was adopted in the subsequent experiment. The optimization of aptamer concentration and the incubation time between the aptamer and target detection MC-LR are discussed in the supplementary materials.

FL characterization of the ZnTCPP@MOF and the construction of aptasensor

The details of the construction of a FL aptasensor are shown in Scheme 1 and characterized by FL spectrum

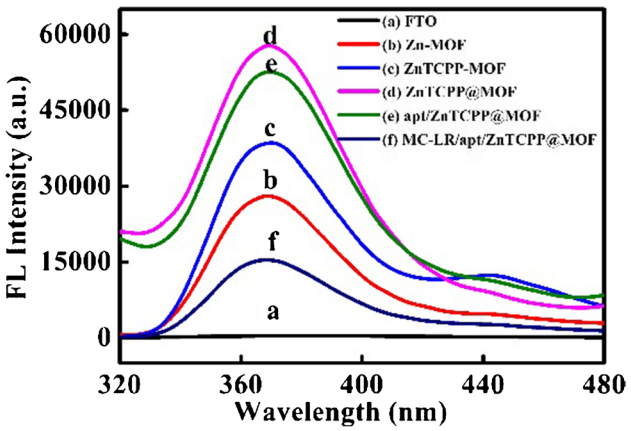

Fig. 5 Fluorescence spectrum of bare FTO (a), Zn-MOF/FTO (b), ZnTCPP-MOF/FTO (c), ZnTCPP@MOF/FTO (d), apt/ZnTCPP@MOF/FTagenO (e), and MC-LR/apt/ZnTCPP@MOF/FTO; the ultimate concentration of MC-LR was 1.0×10^{-5} M (f). The excitation wavelength was 310 nm, and the slit width was 5 nm

after each step. As shown in Fig. 5, almost no FL intensity was observed at the bare FTO (curve a). When the bare FTO deposited Zn-MOF thin films (curve b), ZnTCPP-MOF thin films (curve c), and ZnTCPP@MOF thin films (curve d), it could be seen that the FL intensity increased gradually and the FL intensity of ZnTCPP@MOF/FTO reached the highest. These results confirm that the ZnTCPP@MOF films can promote the electron transfer and enable the MOFs to encapsulate more ZnTCPP because of the larger surface area. Then a smaller weak FL intensity was noted after the modification of aptamer, which was due to the aptamer as inert biomacromolecules could hinder the electrode transfer. Finally, the obvious quenching of the FL intensity was observed in the presence of.the MC-LR. The reason was that the specific binding between the aptamer and the MC-LR makes the MC-LR adhere to the surface of the aptamer, while the poor conductivity of the MC-LR

would hinder the electron transmission, thus quenching the fluorescence intensity of ZnTCPP@MOF.

The results indicate that the proposed FL aptasensor was successfully fabricated.

In addition, cyclic voltammetry (CV) and electrochemical impedance spectroscopy (EIS) were tested and characterized for each modification process. As shown in Fig.S5A, the bare FTO (curve a) showed a small redox peaks. After the deposition of Zn-MOF thin film (curve b), the redox peak showed a bigger current peak than bare FTO, which is due to the high conductivity and positive metal ions of MOF. With the deposition of ZnTCPP@MOF on the FTO (curve c), the redox peak was much bigger than Zn-MOF/FTO, demonstrating that the composite nanomaterial may further improve the electroactivity. Similarly, the redox peak gradually decreased with gradual modifications of nonconductive substances aptamer and MC-LR. After the final modification with MC-LR, the peak current was reduced to the minimum during construction. At the same time, the assembly procedure of as-prepared biosensors was monitored using EIS, and the results are displayed in Fig. S5B. The same results between EIS characterization and CV characterization were obtained, indicating that the proposed aptasensor was successfully constructed as expectedly.

Under the optimized conditions, water samples containing different concentrations of MC-LR were incubated with the FL aptasensor to test the developed assay for detection MC-LR. As shown in Fig. 6A, when the concentration of MC-LR in the tested solution decreased, we observed that fluorescence intensity at 368 nm increased positively, indicating that more specific recognition sites of the binging of MC-LR to aptamer could weaken fluorescence intensity. A plot of the decreased fluorescence intensity against the logarithm of MC-LR concentrations exhibited a good linear relationship in the dynamic range of 1.0×10^{-12} M to 1.0×10^{-5} M of MC-LR as shown in Fig. 6B. The linear regression equation is $\Delta I_{FL}=61{,}186.6+4609.5$ LogC (M) with a correlation coefficient (R^2) of 0.994 (C represented the concentration of MC-LR, M), and the detection limit was 3.8×10^{-13} M (S/N = 3), which is more sensitive than reported in other literatures (Table S1).

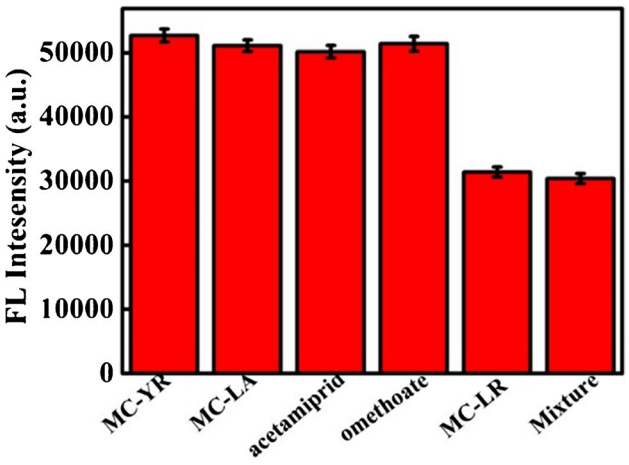

Fig. 7 The FL intensity responses of the aptasensor to 1.0×10^{-7} M MC-YR, 1.0×10^{-7} M MC-LA, 1.0×10^{-7} M acetamiprid, 1.0×10^{-7} M omethoate, and 1.0×10^{-9} M MC-LR and mixture (1.0×10^{-7} M MC-YR + 1.0×10^{-7} M MC-LA + 1.0×10^{-7} M acetamiprid + 1.0×10^{-7} M omethoate + $1.0\times10.^{-9}$ M MC-LR, $n=3$)

To investigate the anti-interference ability of the FL aptasensor, the fluorescence intensities in a mixture system of MC-LR, MC-YR, MC-LA, and other potentially interfering materials (acetamiprid, omethoate) in environmental samples were tested. As shown in Fig. 7, the results exhibited that these interfering agents show much smaller or negligible signals compared to that of target MC-LR, indicating that the prepared FL aptasensor presented excellent selectivity for MC-LR.

The response RSD of 5 sensors in the same batch to 1.0×10^{-10} M MC-LR was 4.2%, and the response RSD of 5 sensors in different batches to 1.0×10^{-10} M MC-LR was 3.2%, which showed the reproducibility of the aptasensor. Fig. S6. also presented the storage lifetime of the developed aptasensor.

To estimate the feasibility and practicability of the aptasensor in actual analysis, we also analyzed the MC-LR levels in water from ponds by the standard addition. As shown in Table S2, the average recovery values ranged from 96 to 104%, along with the RSD of 4.1%. We also used the LC–MS method

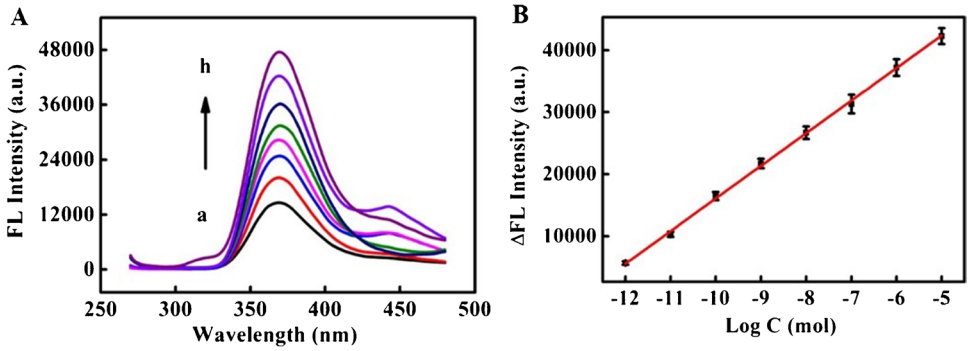

Fig. 6 **A** Fluorescence emission spectrum of curve diagram and **B** the corresponding linear relationship diagram of different concentrations of MC-LR. PBS, 0.1 M pH 7.5; MC-LR concentration from a to g: 1.0×10^{-5} M (a), 1.0×10^{-6} M (b), 1.0×10^{-7} M (c), 1.0×10^{-8} M (d), 1.0×10^{-9} M (e), 1.0×10^{-10} M (f), 1.0×10^{-11} M (g), $1.0\times10.^{-12}$ M (h)

to demonstrate the accuracy of the ECL method; the recovery rate of acetamiprid in the pond water was between 98 and 104%, and the RSD of the measured value was 3.0%. These satisfactory results indicated that the prepared aptasensor possessed good reliability and potential applicability for the determination of MC-LR detection in water samples.

Conclusion

In this work, a novel, simple, and one-step electrochemical method for in situ constructing ZnTCPP-functionalized MOF thin films was developed for selective detection of MC-LR in pond water. ZnTCPP@MOF thin films could be deposited on the electrode surface in situ during the synthesis process. The ZnTCPP@MOF films, as a sensor platform, present an excellent FL behavior due to that massive ZnTCPP molecules are encapsulated in the frameworks. On the basis of the interaction between aptamers with MC-LR, the ZnTCPP@MOF films can achieve a unique FL aptasensor with excellent sensitivity, specificity, and a very low LOD in MC-LR detection. In summary, this work is an alternative for typical FL analytical strategies and opens new ways for synthesis of FL intensity-functionalized MOF materials for applications in FL aptasensor. This developed FL aptasensor can be applied in practical environment. Of course, the electrochemical deposition method is not applicable to all MOFs, and it is worth further research.

Supplementary information The online version contains supplementary material available at https://doi.org/10.1007/s00604-023-05711-4.

Acknowledgements The authors are grateful to the financial support provided by the National Natural Science Foundation of China (No. 22178031, 51874050, and 21904014), the Natural Science Foundation of Jiangsu Province (BK20190928), and the Foundation of Jiangsu Key Laboratory of Advanced Catalytic Materials and Technology (BM2012110).

Declarations

Conflict of interest The authors declare no competing interests.

References

1. Zhang L, Dong H, Li H, Li B, Zhao G, Cai H, Chen L, Dong J (2021) Novel signal-on immunosensors for rapid and sensitive detection of Microcystin-LR. Microchem J 167:106295. https://doi.org/10.1016/j.microc.2021.106295
2. Lei LM, Wu YS, Gan NQ, Song LR (2004) An ELISA-like time-resolved fluorescence immunoassay for microcystin detection. Clin Chim Acta 348(1–2):177–180. https://doi.org/10.1016/j.cccn.2004.05.019
3. Liu Y, Li B, Zhang H, Liu Y, Xie P (2022) Participation of fluorescence technology in the cross-disciplinary detection of microcystins. Coord Chem Rev 457:214416. https://doi.org/10.1016/j.ccr.2022.214416
4. Moura DS, Pestana CJ, Moffat CF, Hui J, Irvine JTS, Edwards C, Lawton LA (2022) Adsorption of cyanotoxins on polypropylene and polyethylene terephthalate: microplastics as vector of eight microcystin analogues. Environ Pollut 303:119135. https://doi.org/10.1016/j.envpol.2022.119135
5. Pang P, Teng X, Chen M, Zhang Y, Wang H, Yang C, Yang W, Barrow CJ (2018) Ultrasensitive enzyme-free electrochemical immunosensor for microcystin-LR using molybdenum disulfide/gold nanoclusters nanocomposites as platform and Au@Pt core-shell nanoparticles as signal enhancer. Sens Actuators, B Chem 266:400–407. https://doi.org/10.1016/j.snb.2018.03.154
6. Calado SLM, Vicentini M, Santos GS, Pelanda A, Santos H, Coral LA, Magalhaes VF, Mela M, Cestari MM, Silva de Assis HC (2019) Sublethal effects of microcystin-LR in the exposure and depuration time in a neotropical fish: multibiomarker approach. Ecotoxicol Environ Saf 183:109527. https://doi.org/10.1016/j.ecoenv.2019.109527
7. Shahmohamadloo RS, Ortiz Almirall X, Simmons DBD, Poirier DG, Bhavsar SP, Sibley PK (2022) Fish tissue accumulation and proteomic response to microcystins is species-dependent. Chemosphere 287:132028. https://doi.org/10.1016/j.chemosphere.2021.132028
8. Qian ZY, Li ZG, Ma J, Gong TT, Xian QM (2017) Analysis of trace microcystins in vegetables using matrix solid-phase dispersion followed by high performance liquid chromatography triple-quadrupole mass spectrometry detection. Talanta 173:101–106. https://doi.org/10.1016/j.talanta.2017.05.079
9. Akyol C, Ozbayram EG, Accoroni S, Radini S, Eusebi AL, Gorbi S, Vignaroli C, Bacchiocchi S, Campacci D, Gigli F, Farina G, Albay M, Fatone F (2021) Monitoring of cyanobacterial blooms and assessing polymer-enhanced microfiltration and ultrafiltration for microcystin removal in an Italian drinking water treatment plant. Environ Pollut 286:117535. https://doi.org/10.1016/j.envpol.2021.117535
10. Campas M, Szydlowska D, Trojanowicz M, Marty JL (2005) Towards the protein phosphatase-based biosensor for microcystin detection. Biosens Bioelectron 20(8):1520–1530. https://doi.org/10.1016/j.bios.2004.06.002
11. Li X, Cheng R, Shi H, Tang B, Xiao H, Zhao G (2016) A simple highly sensitive and selective aptamer-based colorimetric sensor for environmental toxins microcystin-LR in water samples. J Hazard Mater 304:474–480. https://doi.org/10.1016/j.jhazmat.2015.11.016
12. Zhang H, Yang S, Beier RC, Beloglazova NV, Lei H, Sun X, Ke Y, Zhang S, Wang Z (2017) Simple, high efficiency detection of microcystins and nodularin-R in water by fluorescence polarization immunoassay. Anal Chim Acta 992:119–127. https://doi.org/10.1016/j.aca.2017.09.010
13. Li M, Lin H, Paidi SK, Mesyngier N, Preheim S, Barman I (2020) A fluorescence and surface-enhanced raman spectroscopic dual-modal aptasensor for sensitive detection of cyanotoxins. ACS Sens 5(5):1419–1426. https://doi.org/10.1021/acssensors.0c00307
14. Huang H, Li S, Chen B, Wang Y, Shen Z, Qiu M, Pan H, Wang W, Wang Y, Li X (2022) Endoplasmic reticulum-targeted polymer dots encapsulated with ultrasonic synthesized near-infrared carbon nanodots and their application for in vivo monitoring of Cu(2). J Colloid Interface Sci 627:705–715. https://doi.org/10.1016/j.jcis.2022.07.095
15. Su C, Song Q, Jiang D, Dong C, Shan X, Chen Z (2021) An electrochemiluminescence aptasensor for diethylstilbestrol assay based on resonance energy transfer between Ag3PO4-Cu-MOF(II) and silver nanoparticles. Analyst 146(13):4254–4260. https://doi.org/10.1039/d1an00599e

16. Bostan HB, Taghdisi SM, Bowen JL, Demertzis N, Rezaee R, Panahi Y, Tsatsakis AM, Karimi G (2018) Determination of microcystin-LR, employing aptasensors. Biosens Bioelectron 119:110–118. https://doi.org/10.1016/j.bios.2018.08.003
17. Bilibana MP, Citartan M, Fuku X, Jijana AN, Mathumba P, Iwuoha E (2022) Aptamers functionalized hybrid nanomaterials for algal toxins detection and decontamination in aquatic system: current progress, opportunities, and challenges. Ecotoxicol Environ Saf 232:113249. https://doi.org/10.1016/j.ecoenv.2022.113249
18. Gu C, Liu Y, Hu B, Liu Y, Zhou N, Xia L, Zhang Z (2020) Multicomponent nanohybrids of nickel/ferric oxides and nickel cobaltate spinel derived from the MOF-on-MOF nanostructure as efficient scaffolds for sensitively determining insulin. Anal Chim Acta 1110:44–55. https://doi.org/10.1016/j.aca.2020.03.019
19. Li L, Zhao Y, Li X, Ma H, Wei Q (2019) Label-free electrochemiluminescence immunosensor based on Ce-MOF@g-C3N4/Au nanocomposite for detection of N-terminal pro-B-type natriuretic peptide. J Electroanal Chem 847:113222. https://doi.org/10.1016/j.jelechem.2019.113222
20. Li Z, Cui J, Liu Y, Li J, Liu K, Shao M (2018) Electrosynthesis of well-defined metal-organic framework films and the carbon nanotube network derived from them toward electrocatalytic applications. ACS Appl Mater Interfaces 10(40):34494–34501. https://doi.org/10.1021/acsami.8b12854
21. Li M, Dinca M (2011) Reductive electrosynthesis of crystalline metal-organic frameworks. J Am Chem Soc 133(33):12926–12929. https://doi.org/10.1021/ja2041546
22. Ji H, Hwang S, Kim K, Kim C, Jeong NC (2016) Direct in situ conversion of metals into metal-organic frameworks: a strategy for the rapid growth of MOF films on metal substrates. ACS Appl Mater Interfaces 8(47):32414–32420. https://doi.org/10.1021/acsami.6b12755
23. Caddeo F, Vogt R, Weil D, Sigle W, Toimil-Molares ME, Maijenburg AW (2019) Tuning the size and shape of nanoMOFs via templated electrodeposition and subsequent electrochemical oxidation. ACS Appl Mater Interfaces 11(28):25378–25387. https://doi.org/10.1021/acsami.9b04449
24. Liu J, Woll C (2017) Surface-supported metal-organic framework thin films: fabrication methods, applications, and challenges. Chem Soc Rev 46(19):5730–5770. https://doi.org/10.1039/c7cs00315c
25. Azhar MR, Hussain G, Tade MO, Silvester DS, Wang S (2020) Electrodeposited metal organic framework toward excellent hydrogen sensing in an ionic liquid. ACS Appl Nano Mater 3(5):4376–4385. https://doi.org/10.1021/acsanm.0c00503
26. Sun Z, Peng Y, Wang M, Lin Y, Jalalah M, Alsareii SA, Harraz FA, Yang J, Li G (2021) Electrochemical deposition of Cu metal-organic framework films for the dual analysis of pathogens. Anal Chem 93(25):8994–9001. https://doi.org/10.1021/acs.analchem.1c01763
27. Alizadeh S, Nematollahi D (2017) Electrochemically assisted self-assembly technique for the fabrication of mesoporous metal-organic framework thin films: composition of 3D Hexagonally packed crystals with 2D honeycomb-like mesopores. J Am Chem Soc 139(13):4753–4761. https://doi.org/10.1021/jacs.6b12564
28. Yoneda T, Sung YM, Lim JM, Kim D, Osuka A (2014) Pd(II) complexes of [44]- and [46]decaphyrins: the largest Huckel aromatic and antiaromatic, and Mobius aromatic macrocycles. Angew Chem Int Ed Engl 53(48):13169–13173. https://doi.org/10.1002/anie.201408506
29. Pushpanandan P, Ravikanth M (2021) Neo-porphyrinoids: new members of the porphyrinoid family. Top Curr Chem (Cham) 379(4):26. https://doi.org/10.1007/s41061-021-00338-6
30. Chen J, Zhu Y, Kaskel S (2021) Porphyrin-based metal-organic frameworks for biomedical applications. Angew Chem Int Ed Engl 60(10):5010–5035. https://doi.org/10.1002/anie.201909880
31. Shang S, Xiong W, Yang C, Johannessen B, Liu R, Hsu H-Y, Gu Q, Leung MKH, Shang J (2021) Atomically dispersed iron metal site in a porphyrin-based metal–organic framework for photocatalytic nitrogen fixation. ACS Nano 15(6):9670–9678. https://doi.org/10.1021/acsnano.0c10947
32. Yu K, Lee Y-R, Seo JY, Baek K-Y, Chung Y-M, Ahn W-S (2021) Sonochemical synthesis of Zr-based porphyrinic MOF-525 and MOF-545: enhancement in catalytic and adsorption properties. Microporous Mesoporous Mater 316:110985. https://doi.org/10.1016/j.micromeso.2021.110985
33. NgongangNdjawa GO, Tchalala MR, Shekhah O, Khan JI, Mansour AE, Czaban-Jozwiak J, Weselinski LJ, AitAhsaine H, Amassian A, Eddaoudi M (2019) The growth of photoactive porphyrin-based MOF thin films using the liquid-phase epitaxy approach and their optoelectronic properties. Materials (Basel) 12(15):2457. https://doi.org/10.3390/ma12152457
34. Zhao J, Liu X, Wu Y, Li D-S, Zhang Q (2019) Surfactants as promising media in the field of metal-organic frameworks. Coord Chem Rev 391:30–43. https://doi.org/10.1016/j.ccr.2019.04.002
35. Qin X, Zhang X, Wang M, Dong Y, Liu J, Zhu Z, Li M, Yang D, Shao Y (2018) Fabrication of Tris(bipyridine)ruthenium(II)-functionalized metal-organic framework thin films by electrochemically assisted self-assembly technique for electrochemiluminescent immunoassay. Anal Chem 90(19):11622–11628. https://doi.org/10.1021/acs.analchem.8b03186
36. Su Z, Tang D, Liu J, Yang X, Xu S, Xu W, Zhou Y, Xu M, Yi J, Jiang H, Shao Y, Qin X (2021) Electrochemically-assisted deposition of toluidine blue-functionalized metal-organic framework films for electrochemical immunosensing of Indole-3-acetic acid. J Electroanal Chem 880:114855. https://doi.org/10.1016/j.jelechem.2020.114855
37. Li M, Dincă M (2014) Selective formation of biphasic thin films of metal–organic frameworks by potential-controlled cathodic electrodeposition. Chem Sci 5(1):107–111. https://doi.org/10.1039/c3sc51815a